Scalable Production of Edge-Functionalized Graphene Nanoplatelets via Mechanochemical Ball-Milling

In-Yup Jeon, Seo-Yoon Bae, Jeong-Min Seo, and Jong-Beom Baek**

Although there are a variety of methods for producing graphene, commercialization remains challenging because each method has its own pros and cons. For the wide use of graphene as a next generation material in diverse applications, the process by which graphene is manufactured must be robust enough to overcome barriers to commercialization, as has been experienced in commercializing carbon nanotube products. Here, a recent discovery of a new manufacturing process for efficient delamination of graphite into graphene nanoplatelets (GnPs) via mechanochemical ball-milling is summarized. In this process, transferring sufficient kinetic energy to graphitic frameworks will crack graphitic C–C bonds, generate active carbon species (mostly carbon free radicals), introduce edge-functional groups, and delaminate graphitic layers into edge-functionalized GnPs (EFGnPs). While this process is a method for mass production, it does not involve hazardous chemicals (e.g., corrosive acids and toxic reducing agents) such as those used for producing graphene oxide (GO) and reduced graphene oxide (rGO). Owing to its edge-selective functionalization, the EFGnPs have minimal basal area defects with selectivity of a variety of edge groups by forming edge C–X bonds (X = nonmetals or metalloids) that are tunable.

1. Introduction

Graphene is a 2D sheet of sp^2-hybridized, networked carbon.. Its extended honeycomb graphitic framework is the basic building block for other important carbon allotropes. It can be stacked into 3D graphite, rolled to form 1D nanotubes, and wrapped to form 0D fullerenes. Its unique physical, mechanical and electrical properties have drawn great interest among scientists.[1–4] Among these are its large theoretical specific surface area (2630 $m^2\ g^{-1}$), high intrinsic mobility (200 000 $cm^2\ v^{-1}\ s^{-1}$), high Young's modulus (≈1.0 TPa) and thermal conductivity (≈5000 $W\ m^{-1}\ K^{-1}$), good optical transmittance (≈97.7%), and good electrical conductivity. As a result, graphene has been considered to be a promising candidate for composite additives,[5,6] transparent conducting electrodes,[7,8] field effect transistors,[9] photovoltaic cells,[10,11] fuel cells,[12,13] Li-ion batteries,[14,15] sensors,[16] supercapacitors,[17] and many others.

Dr. I.-Y. Jeon, S.-Y. Bae, J.-M. Seo, Prof. J.-B. Baek
School of Energy and Chemical Engineering
Center for Dimension-Controllable Organic Frameworks
Ulsan National Institute of Science and Technology (UNIST), 50, UNIST
Ulsan 689–798, Korea
E-mail: inyup@unist.ac.kr; jbbaek@unist.ac.kr

DOI: 10.1002/adfm.201502214

Since the direct isolation of single-layer graphene from graphite was successfully realized by mechanical exfoliation—the so-called "Scotch tape" method,[1]—and potential applications demonstrated, graphene has been produced in several ways. These techniques involve graphite-intercalation compounds (GICs),[18] electrochemical exfoliation,[19] chemical oxidation/reduction (or graphite oxide (GO)/reduced graphene oxide (rGO)),[20,21] arc discharge exfoliation,[22] epitaxial growth on SiC,[23] and chemical vapor deposition (CVD).[8,24] Among these, the GO/rGO and CVD approaches have mainly been utilized for the synthesis of graphene for mass and high-quality production, respectively. When the GO/rGO and CVD methods are compared, they can be clearly categorized on the basis of graphene quality and applications.

Although CVD is one of the most viable methods for the formation of large-area and high-quality graphene film,[7,8] it has significant drawbacks that include a tedious manufacturing process, high manufacturing costs, and quality control issues. Therefore, CVD graphene will be useful for only limited applications such as transparent electrodes and field effect transistors. Compared with mechanically exfoliated and CVD graphene, GO/rGO has relatively poor quality, but it is considered mass producible at low-cost. Specifically, it is possible to produce affordable quantities to use for energy conversion and storage, catalysts, composites, and flame retardants. However, GO/rGO production is associated with many problems such as low-quality, use of hazardous reagents (e.g., strong acids and carcinogenic reducing agents), and a tedious process. Although there are many limitations for commercialization of graphene, both GO/rGO and CVD are still regarded as the most viable approaches for practical uses. Nevertheless, they are not adequate for commercial demands, and thus many scientists have worked hard to find alternatives that would allow scalable production of high-quality graphene and/or graphene nanoplatelets (GnPs, less than 10 graphitic layers), using a simple, cost-efficient, eco-friendly, and mass producible process. At the same time, the quality of the graphene and GnPs produced should be good enough to meet commercial demands.

We recently reported a new approach for scalable production of graphene nanoplatelets (GnPs), which involves simple but efficient production via mechanochemical ball-milling graphite in the presence of corresponding reactants.[25] High-speed

ball-milling generates enough kinetic energy to crack graphitic C–C bonds, to induce edge reaction, to delaminate graphitic layers, and thus to yield edge-selectively functionalized graphene nanoplatelets (EFGnPs). Large quantities of EFGnPs could be efficiently prepared by mechanochemical ball-milling. Due to the minimal distortion of the graphitic basal area, EFGnPs have high crystallinity and show excellent performance in a number of applications (e.g., fuel cells,[26–31] solar cells,[32–35] Li-ion batteries,[32,36] and flame retardants.[37] In addition, a variety of functional groups and/or heteroatoms can be selectively introduced at the edges for different applications. Hence, this EFGnPs approach may thoroughly satisfy diverse demands and overcome previous obstacles to commercialization. We believe that this process could revitalize graphene research for practical applications (e.g., polymer composites, energy conversion and storage, flame retardants, conductive inks) and thus enable graphene to take an actual leading position as a next-generation material in future science and technology.

2. Mechanochemically Driven Reaction using Kinetic Energy (Ball-Milling)

As a new method for large-quantity and high-quality production of GnPs, a mechanochemical reaction was developed utilizing ball-milling. Such ball-milling utilizes metal balls travelling at high speed (significant kinetic energy) to unzip the graphitic layers (C–C bond cracking), cause chemical reaction at the unzipped edges (C–X bond formation), and physically delaminating graphitic layers into GnPs (<10 layers). Chemically bonded X groups act as physical wedges, hampering the restacking of the separated GnPs. As presented in **Figure 1**, the bond cleavages of graphitic C–C frameworks are induced by the high-energy metal balls in a planetary ball-mill machine (Figure 1a). Active carbon species such as carbon radicals and ions (cations and anions) are generated at the unzipped edges. Active carbon species generated in situ are reactive enough to promptly pick up appropriate reactants that are present (Figure 1b–d). The reactants can be in different phases: vapors (CO_2,[25] N_2,[28] F_2[32] and Cl_2[27]), liquids (SO_3[26] and Br_2,[27] solids (I_2,[27] red P,[37] S_8[29] and Sb,[31] or mixtures (CO_2/SO_3[26] and SO_3/I_2[30] under standard conditions. When the ball-mill capsule lid is opened in ambient air, violent sparking could be observed due to the termination/oxidation reaction between the remnant active carbon species/metallic debris and the moisture in the air.[25,27] After acidic work-up to remove metallic residue, the EFGnPs contain some oxygenated functional groups (e.g., –OH, –C=O, –COOH) at their edges along with the appropriate reactants. The polar edge-oxygenated groups help solubility of EFGnPs in solvents (vide infra), allowing enhanced processibility.

Considering the whole manufacturing process, the major advantages of the ball-milling approach to produce GnPs (over the GO/rGO method) are: 1) very simple, one-pot eco-friendly process without use of hazardous wet-chemicals; 2) efficient way to selectively introduce various functional groups; 3) minimal distortion at basal area for high-quality materials (**Table 1**). The process for making EFGnPs only involves milling and work-up procedures along with the diversification of reactants, in contrast with the tedious GO/rGO process (oxidation, sonication, separation, fabrication, and reduction). After milling, it is only necessary for EFGnPs to be treated with 1 M aq. HCl solution to remove the metallic debris incorporated during ball-milling. Namely, there is no need for additional processes

In-Yup Jeon is a post-doctoral research fellow in the School of Energy and Chemical Engineering/Center for Dimension-Controllable Organic Frameworks, Ulsan National Institute of Science and Technology (UNIST), South Korea. He received his PhD degree in Energy Engineering from UNIST in 2013. His research interests are the edge-selective functionalization of carbon-based materials for energy conversion and storage.

Jeong-Min Seo is a PhD candidate in School of Energy & Chemical Engineering/Center for Dimension-Controllable Organic Frameworks, Ulsan National Institute of Science and Technology (UNIST), South Korea. She received her B.S. degree in Fine Chemical Engineering and Applied Chemistry from Chungnam National University in 2011. Her current research work is related to design, synthesis and application of covalent-organic frameworks (COFs) and porous organic polymers.

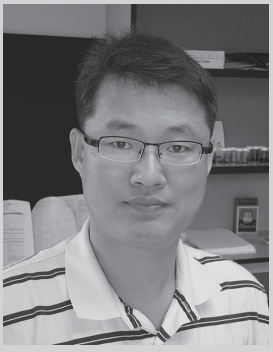

Jong-Beom Baek is a Professor of School of Energy & Chemical Engineering at the Ulsan National Institute of Science and Technology (UNIST), South Korea. After receiving his PhD in Polymer Science from the University of Akron (USA) in 1998, he joined the Wright-Patterson Air Force Research Laboratory (AFRL). After four years at the AFRL, he returned to Korea as an Assistant Professor of Chemical Engineering at Chungbuk National University (Korea) in 2003, before moving to UNIST in 2008. His current research interests are the syntheses of high-performance covalent organic frameworks and the chemical modifications of carbon-based materials for multifunctional applications.

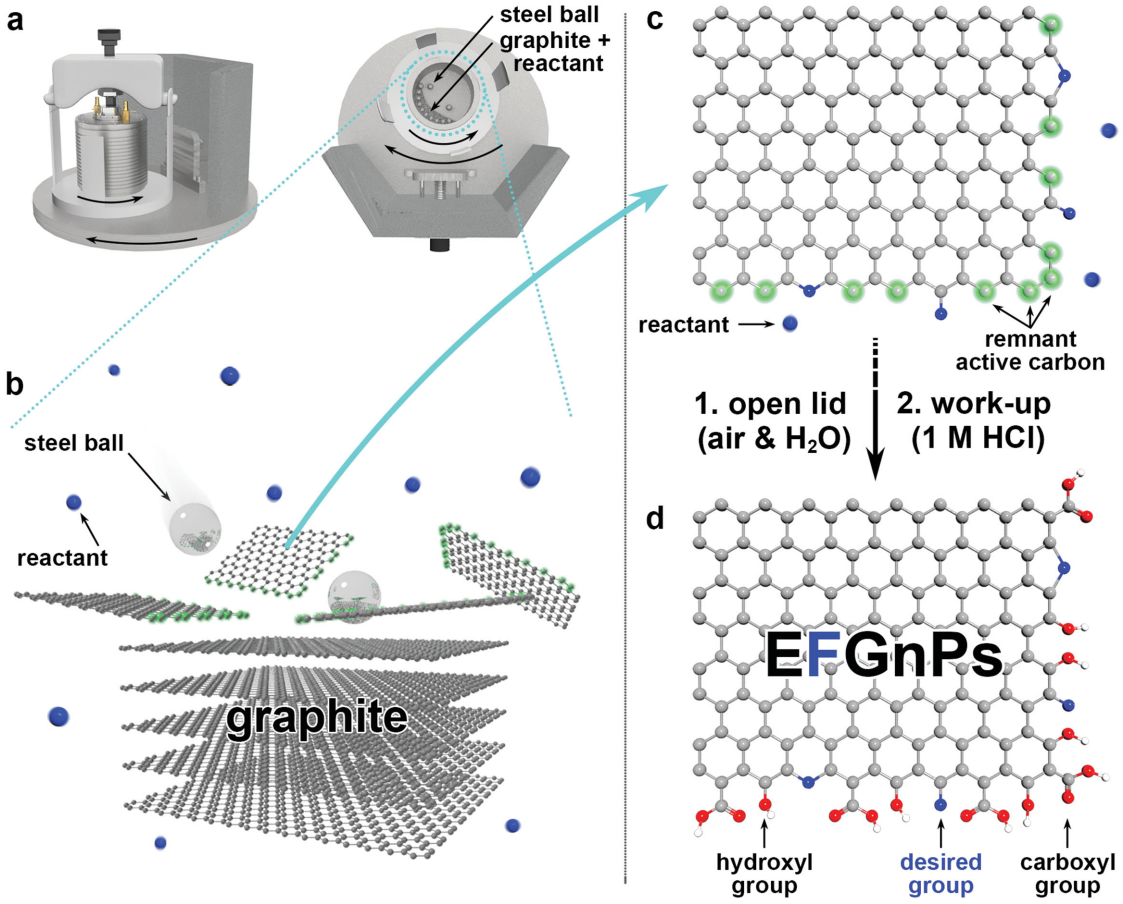

Figure 1. a) Planetary ball-mill machine; b–d) schematic representation of the mechanochemically driven physical cracking, and chemical reaction by ball-milling graphite in the presence of corresponding reactant(s) to produce edge-selectively functionalized graphene nanoplatelets (EFGnPs) with desired functional group(s).

such as reduction, transfer, or etching. Therefore, a very simple manufacturing process, along with the low-cost installation of ball-milling devices, could lower the production cost of the commercialization of graphene.

3. Edge-Selectivity of EFGnPs

The edge-selectivity was indirectly confirmed by focused micro-Raman spectra.[25] The I_D/I_G ratio of EFGnPs was noticeably different between edge and basal plane (**Figure 2**a). The carboxylic acid-functionalized graphene nanoplatelets (CGnPs) showed a much higher I_D/I_G ratio (1.32) at edges than the corresponding value (0.33) for the basal plane. While pristine graphite exhibits a similar trend (Figure 2b), GO (Figure 2c), which has oxygenated groups at both edges and in the basal area, displays a similar I_D/I_G ratio of the edges and basal area. In addition, CGnPs display sp^3 peaks (1134 cm^{-1}) at the edges (arrow, Figure 2a), while both the pristine graphite and GO do not show the sp^3 peak. The Raman results suggest edge-selective functionalization of EFGnPs.

Furthermore, the edge-selectivity was visually elucidated by atomic resolution transmission electron microscopy (AR-TEM). Because the atomic sizes of carbon (covalent radius: 73 pm), nitrogen (71 pm) and oxygen (66 pm) are similar, the electron microscope cannot discern the elements. To directly visualize edge-selectivity, we introduced antimony (Sb, 139 pm) at the edges of the graphene nanoplatelets (GnPs), in other words, we prepared antimony-doped graphene nanoplatelets (SbGnPs).[31] A high-resolution TEM (HR-TEM) image shows thin SbGnP platelets (Figure 2d), and the AR-TEM image clearly displays the formation of C–Sb bonds along the edges of SbGnPs (Figure 2e). The Sb atoms with dark atomic contrast are located along the edge lines of the SbGnPs. A HAADF STEM image (Figure 2f) with atomic Z-contrast, confirms the existence of a single Sb atom without formation of Sb nanoparticles. Furthermore, due to the large atomic size of Sb, it is attached at the armchair edge of SbGnPs (Figure 2g). The resulting formation of C–Sb bonds suggest that high-speed ball-milling of graphite and antimony ore could generate sufficient kinetic energy for the formation of graphitic C–X bonds regardless of the reactants used (X = nonmetals or metalloids).

Furthermore, the total number of active carbon species generated at the broken edges of graphitic layers can be estimated by Eq. (1).[37]

$$8a\sum_{k=1}^{n}\left(\frac{1}{2}\right)^{k}\cdot 4^{k-1}=2a\sum_{k=1}^{n}2^{k} \quad (1)$$

Table 1. Comparison of general characteristics of EFGnP and GO.[25]

	EFGnP	GO	Advantages for EFGnP
History	2011: Invention	1860: Brodie	GO has known for longer than 150 years
		1898: Staudenmaier	
		1958: Hummers	
Reactant	Graphite + CO_2	Graphite + $NaNO_3$, $KMnO_4$, H_2SO_4	EFGnP is an eco-friendly process
Yield	Very high (quantitative)	Low	Only limited by the size of the ball milling chamber
Interlayer d-spacing (Å)	3.7	≈6.67–7.70	Graphite = 3.4
C/O ratio	3.63	2.25	timeless C-basal plane damage
I_D/I_G ratio	1.15	1.03	Depending on reaction time
Functional groups	Carboxylic acid only	Various (carboxylic acid, carbonyl, aldehyde, epoxy, hydroxyl, etc.)	Well-defined functional groups could be further selectively modified by using carboxylic acid reaction
Functional groupselectivity	Selective	Non-selective	Highly selective, but other functional groups can also be selectively introduced via the ball milling process (e.g., amine and sulfonic acid)
Regio-selectivity	Edge only	Edge + basal plane	Region-specific
Powder conductivity (S cm^{-1})	1.1×10^{-2}	6×10^{-7}	Much higher conductivity (Graphite ≈10–1400)
		6.8×10^{-10}	
Char yield at 800 °C in N_2	<65%	<60%	ECG has better thermal stability
Dispersibility in basic solvents	good	good	Higher stable concentration (≈three times in NMP)
Zeta-potential (mV)	–34.2 (NMP)	–35.1 (NMP)	Similar
	–41.6 (water, pH = 10)	–43.0 (water, pH = 10)	

where a is the initial average number of carbon atoms at the edges of the pristine graphite, and k is the number in crosscuts. As a simple model, a square piece of graphene with one hundred carbon atoms (a = 100) on an edge and with three crosscuts (k = 3) can generate 2800 active carbon species (i.e., 2800/10 000 × 100 = 28%), which is sufficient to functionalize and thus affect the overall nature of the EFGnPs.

4. Edge-Tunability of EFGnPs with Various Functional Groups and Heteroatoms

In the case of GO/rGO processes, the type of oxygenated group cannot be specified and its physical location is not selectively defined either at the edges or on the basal plane, since the $NaNO_3/H_2SO_4/KMnO_4$ mixture randomly oxidizes the graphitic framework with a variety of oxygenated groups (e.g., –OH, –O–, –C=O, –COOH) together at the edges and on the basal plane.[38,39] Therefore, GO requires additional chemical reaction and/or heat treatment to functionalize the desired groups, and/or to introduce heteroatoms. Even with this potential, there are still a lot of limitations to imparting specific functional groups and/or heteroatoms. For example, the GO/rGO approach allows only the possibility of nonmetallic elements (e.g., B, N, P, S, I) through chemical reduction and/or heat treatment at high temperature. It is considered to be almost impossible to introduce post-transition metals or metalloids.

On the other hand, the ball-milling process can selectively introduce desired functional groups (e.g., –H, –COOH, $–SO_3H$ and $–P{=}O(OH)_2$) and heteroatoms (N, S, F, Cl, Br, I and Sb) at the edges of EFGnPs. This can be simply realized by changing reactants without additional procedures, as summarized in **Table 2**. Further chemical modification of EFGnPs is also possible. For example, CGnPs (edge-COOH containing GnPs) can be converted to edge-COCl, and subsequently into edge-$CONH_2$ by treating with $SOCl_2$ followed by ammonia.[40] In addition, polymers can be grafted to the edges of CGnPs using esterification.[41] Very recently, the formation of graphitic C–Sb bonds has, for the first time, been realized using ball-milling of graphite and antimony (Sb) ore.[31] The result suggests that ball-milling generates enough kinetic energy to initiate chemical reaction between active carbon species and various other chemical species, and to form graphitic C–X bonds (X = nonmetals, metalloids, post-transition metals or metals) that have not yet been reported elsewhere. Thus, new challenges for the formation of graphitic C–X bonds could open new avenues for controlling the structure-property relationship. This has not been possible with other synthesis methodologies; hence, the potential applications of GnPs will be beyond our imagination.

5. Solubility and Average Aumber of Aayers of EFGnPs

EFGnPs are generally dispersible well in polar solvents such as water, alcohol, tetrahydrofuran (THF), acetone, *N,N*-dimethylformamide (DMF), *N,N*-dimethylacetamide (DMAc), and *N*-methyl-2-pyrrodine (NMP), indicating that the driving force for the good dispersion stability must originate from edge polarity (enthalpic contribution) and grain size reduction (entropic contribution) in addition to the steric repulsion at the edges. This allows small molecules (solvent molecules) to intercalate between graphitic

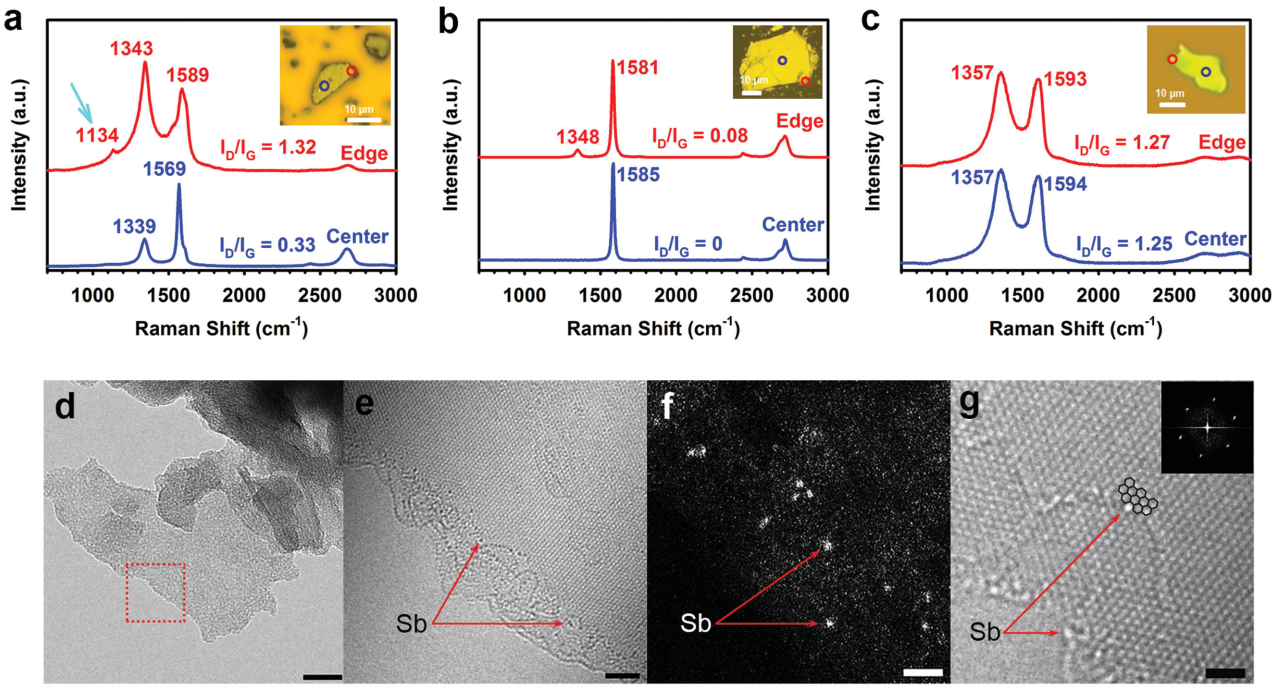

Figure 2. a–c) Indirect validation of edge-selective functionalization using micro-Raman spectra: a) CGnPs after ball-milling for 24 h; b) Pristine graphite; c) GO. Insets are confocal optical microscopy images of the D and G bands. Reproduced with permission.[25] Copyright 2012, National Academy of Sciences; d–g) Direct validation of edge-selective functionalization using TEM: d) Bright-field (BF) TEM image of SbGnPs after ball-milling. Scale bar is 20 nm; e) Atomic-resolution (AR) TEM image obtained from the region marked with a red square in (d). Scale bar is 2 nm; f) HAADF STEM image showing the contrast of single Sb atoms at the edges of SbGnPs. Scale bar is 1 nm; g) AR-TEM image of a single Sb atom attached at the graphene edge with an armchair configuration. The inset is the fast Fourier transform (FFT) of the image. Scale bar is 1 nm. Reproduced with permission.[31] Copyright 2015, Nature Publishing Group.

EFGnPs layers. As a result, EFGnPs solutions in various solvents show zeta-potential values >–30 mV (**Table 3**), implying an absolute value higher than ±30 mV for a stable dispersion.[42,43] Thus, the enhanced solubility of EFGnPs in various solvents can be attributed not only to various functional groups and/or heteroatoms, but also to some oxygenated groups at their edges. These are unintentionally introduced by the reaction between the remnant active carbon species and air moisture, which turns out to be useful for solution processing.

The average number of layers in solid state EFGnPs after ball-milling could simply be estimated on the basis of their surface area. Given that the maximum Brunauer–Emmett–Teller (BET) surface area of single layer graphene is 2630 $m^2 g^{-1}$, the average numbers of EFGnPs could be calculated by simple dividing the surface area of a single layer by the experimentally determined BET surface areas of EFGnPs. That is, the average number of layers is 2630/BET surface area of corresponding EFGnPs. This is possible because the edge contribution of the graphene nanoplatelets (GnPs) is negligible with respect to the basal area. The estimated average number of EFGnP layers is in the range of ≈4–24 (**Table 4**) in solid state. However, it is noteworthy that further delamination of EFGnPs occurs upon dispersion in solvents, because edge-lifting can provide efficient kinetics for the intercalation of solvent molecules. Furthermore, as the atomic size of edge-substituent increases (for example, in the order F < Cl < Br < I), the BET surface area is accordingly increased, as the average number of layers is decreased. The results indicate that atom size is an important factor in the delamination of graphitic layers in solid state. EFGnPs containing polar edge groups, such as CSGnPs, SGnPs, and ISGnPs that contain sulfonic acid, show very low BET surface area (similar to pristine graphite: 2 $m^2 g^{-1}$). This is because of the relatively larger grain size (SEM morphology) and tighter aggregates caused by stronger surface interactions (H-bonding) between the sulfonic acids on the edges.

6. Applications of EFGnPs

Graphene has received such tremendous attention due to its outstanding chemical, physical, mechanical, optical, and electronic properties. For example, the electron accepting/donating ability of heteroatom-doped graphene can create net positive or negative charges on adjacent carbon atoms in the graphitic lattice to efficiently facilitate electrocatalytic activity.[44] In the case of EFGnPs, heteroatoms are located at the edges where most catalytic activity occurs. Edge-selective doping of functional groups/heteroatoms could play a pivotal role in the overall enhancement of electrocatalytic performance for electrochemical energy conversion and storage.

We have studied various EFGnPs as electrode materials for energy conversion and storage, involving such as fuel cells,[26–31] dye-sensitized solar cells (DSSCs),[32–35] lithium-ion batteries (LIBs),[32,36] and vanadium redox-flow batteries (VRFBs).[45] EFGnPs have demonstrated excellent electrochemical performance with cycle stability. In addition, graphene phosphonic acid (GPA) showed great potential as a flame

Table 2. Yield (starting with 5 g of graphite) and element content of EFGnPs from XPS.

Sample	Yield (g)	C (at.%)	O (at.%)	X (at.%)
HGnP	5.32	89.68	10.32	–
CGnP	6.28	82.22	17.78	–
CSGnP	5.23	86.66	10.69	2.65 (S)
SGnP	5.03	88.52	7.47	4.01 (S)
NGnP	5.67	77.08	13.38	8.47 (N)
SGnP-S_8	5.75	86.99	8.07	4.94 (S)
GPA	10.17	45.82	39.40	14.78 (P)
FGnP	5.15	87.94	12.06	3.00 (F)
ClGnP	6.09	89.09	7.54	3.37 (Cl)
BrGnP	6.93	90.99	6.01	2.99 (Br)
IGnP	6.86	91.36	7.58	1.06 (I)
ISGnP	4.57	83.55	13.17	0.16 (I) and 1.50 (S)
MAGnP	6.45	89.47	10.53	-
MIGnP	7.09	87.99	9.05	2.96 (N)
SbGnP	6.11	82.87	15.95	1.18 (Sb)

HGnP: Hydrogen-functionalized graphene nanoplatelets; CGnP: carboxylic acid-functionalized graphene nanoplatelets; CSGnP: carboxylic acid and sulfonic acid-functionalized graphene nanoplatelets; SGnP: sulfonic acid-functionalized graphene nanoplatelets; NGnP: nitrogen-doped graphene nanoplatelets; GPA: graphene phosphonic acid; SGnP–S_8: sulfur(S_8)-doped graphene nanoplatelets; FGnP: fluorine-doped graphene nanoplatelets; ClGnP: chlorine-doped graphene nanoplatelets; BrGnP: bromine-doped graphene nanoplatelets; IGnP: iodine-doped graphene nanoplatelets; ISGnP: iodine and sulfonic acid-functionalized graphene nanoplatelets; MAGnP: maleic acid-functionalized graphene nanoplatelets; MIGnP: maleimide-functionalized graphene nanoplatelets; SbGnP: antimony-doped graphene nanoplatelets.

retardant,[37] which could replace current brominated flame retardants (BFRs) that are bioaccumulative and toxic.[46]

6.1. As Cathode Materials for Oxygen Reduction Reaction (ORR) in Fuel Cells (FCs)

As energy conversion devices, fuel cells possess many advantages over batteries in terms of energy security, low operating cost, stable power generation, fuel choices, clean emissions, and high power conversion efficiency.[47] However, there are two major technical pitfalls, namely manufacturing cost and reliability, which have hampered their commercialization to date. Specifically, the major drawback is related to the kinetically sluggish cathodic oxygen reduction reaction (ORR) compared with the fast anodic hydrogen oxidation reaction (HOR).[48,49] Hitherto, platinum-based materials are the most efficient catalysts. However, along with the high cost of Pt, there are a variety of problems associated with Pt-based electrocatalysts. These include the potential for carbon monoxide poisoning, fuel selectivity, and long-term stability. Therefore, the development of non-precious metal[50,51] and metal-free[52,53] electrocatalysts with high activity has attracted considerable attention. More importantly, practical durability has become one of the most important challenges for development of fuel cells. Among the better candidates, heteroatom-doped carbon materials such as carbon black,[54] carbon nanoparticles,[55] carbon nanotubes,[44] and graphene[12] have been intensively studied as efficient metal-free electrocatalysts for ORR. As summarized in **Table 5**, EFGnPs, a new class of electrocatalysts, displayed enhanced ORR performance and outstanding electrochemical stability due to edge-selective functionalization or heteroatom doping. This suggests potential new insights for the design and synthesis of low-cost and highly durable electrocatalysts in fuel cells.

Table 3. Dispersion and zeta-potential in various solvents of EFGnPs.

Sample	Max concentration [mg mL^{-1}]	Zeta-potential [mV]	Solvent
CGnP	0.06	−30.5	NMP
CSGnP	0.14	−32.8	DMF
SGnP	0.14	−38.8	DMF
NGnP	0.10	−31.9	DMAc
SGnP-S_8	0.10	−33.7	DMF
PGnP	0.60	−33.3	H_2O
FGnP	0.10	−33.5	NMP
ClGnP	0.10	−33.5	DMF
BrGnP	0.10	−31.6	DMF
IGnP	0.10	−34.8	DMF
ISGnP	0.40	−43.4	NMP

A series of EFGnPs, hydrogen (HGnPs), carboxylic acid (CGnPs), sulfonic acid (SGnPs) and carboxylic acid/sulfonic acid (CSGnPs)-functionalized GnPs, were prepared by ball-milling graphite in the presence of H_2, CO_2, SO_3 or CO_2/SO_3 mixture, respectively.[26] The electrocatalytic activities of EFGnPs are closely related to the edge polarity nature in the order of SGnP > CSGnP > CGnP > HGnP > pristine graphite. These results suggest that the kinetic contribution related to oxygen diffusion by edge polarity could also play an important role in ORR, along with the electron accepting/donating capability (thermodynamic contribution) of EFGnPs.

As an extreme challenge, nitrogen can also be introduced at the edges of GnPs by ball-milling graphite in the presence of

Table 4. Surface area, pore volume, pore size, and estimated average number of layers of EFGnPs in solid state.

Sample	Surface area [$m^2\ g^{-1}$]	Pore Volume [mL g^{-1}]	Pore Size [nm]	Average layer number
Graphite	2.8	0.0016	2.27	–
HGnP	437	0.3909	3.58	5.99
CGnP	389	0.1841	1.89	6.75
CSGnP	2.7	0.0136	20.43	–
SGnP	2.9	0.0135	18.62	–
NGnP	109.0	0.0529	1.94	24.13
SGnP-S_8	143.7	0.0715	1.99	18.30
FGnP	134.8	0.3090	9.17	19.51
ClGnP	471.2	0.2205	1.87	5.58
BrGnP	579.4	0.5474	3.78	4.54
IGnP	662.2	0.3413	2.06	3.97
ISGnP	6.0	0.0205	13.58	–
SbGnP	376.7	0.3857	4.10	6.98

Table 5. ORR performance of EFGnPs.

Sample	Electron transfer number (*n*)	Cycle retention	Reference
Pt/C	4.0 at –0.6 V	81.1% after 100 000 cycles	[31]
HGnP	3.0 at –0.6 V	84.3% after 10 000 cycles	[26]
CGnP	2.9 at –0.6 V	60.6% after 100 000 cycles	[26]
CSGnP	2.8 at –0.6 V	99.3% after 100 000 cycles	[26]
SGnP	3.1 at –0.6 V	97.6% after 100 000 cycles	26
NGnP	4.0 at –0.6 V	95.5% after 100 cycles	[28]
SGnP-S_8	3.3 at –0.6 V	–	[29]
SOGnP	3.6 at –0.6 V	–	[29]
ClGnP	3.5 at –0.8 V	95.4% after 100 cycles	[27]
BrGnP	3.8 at –0.8 V	93.2% after 100 cycles	[27]
IGnP	3.9 at –0.8 V	96.2% after 100 cycles	[27]
ISGnP	4.0 at –0.6 V	66.4% after 100 000 cycles	[30]
SbGnP	4.0 at –0.6 V	101.5% after 100 000 cycles	[31]

nitrogen gas.[28] Density functional theory (DFT) calculation of nitrogen-doped GnPs (NGnPs) reveals that the lone-pair states of nitrogen in-plane orbitals constitute distinctive edge-localized bands just below the Fermi-level. However, the π states of graphene are well preserved, including the nitrogen P_z-orbitals in the conjugated networks. These unique edge-localized band structures, in conjunction with the undamaged basal plane of NGnPs, can lead to advantageous catalysts that surpass the performance of Pt. The corresponding cathodic reduction peak for NGnPs is positively shifted and provides a higher a current density (–0.28 V and –0.54 mA cm^{-2}), compared with pristine graphite (–0.43 V and –0.19 mA cm^{-2}). Moreover, the current-density of NGnPs is similar to that of Pt/C. Additionally, NGnPs show an ideal four-electron process and superb stabilities in both N_2- and O_2-saturated electrolytes.

Other series of halogen-doped GnPs (XGnPs, X = Cl, Br or I) were prepared by ball-milling graphite in the presence of Cl_2, Br_2 or I_2, respectively.[27] XGnPs show remarkable electrocatalytic activities toward ORR with high selectivity, good tolerance to methanol crossover/CO poisoning effects, and excellent long-term cycle stability (**Figure 3**). The edges of XGnPs have enough activity to attract O_2 and to weaken the O–O bond of adsorbed O_2, which is favorable for efficient development into water upon reduction and protonation. The origin of enhanced ORR activity with the nitrogen-doped carbon-based materials is due to the higher electronegativity (χ) of nitrogen (3.04, compared to carbon: 2.55) to polarize adjacent carbon atoms in graphitic frameworks. This efficiently facilitates O_2 adsorption and charge-transfer. However, although the order of electronegativity is Cl (3.16) > Br (2.96) > I (2.66), the order of ORR activity of XGnPs is ClGnP << BrGnP < IGnP. This is due to the enhancement of charge-transfer by the formation of partially ionized bonds such as $–Br^+–$ and $–I^+–$ because of their relatively larger atomic sizes.

Sulfur-doped graphene nanoplatelets (SGnP-S_8) were prepared using sulfur (S_8) and then were treated in hydrogen peroxide to oxidize SGnPs-S_8 into SOGnPs.[29] Both SGnPs-S_8 and SOGnPs demonstrate not only high ORR electrocatalytic activity but also better fuel selectivity with longer-term stability than those of pristine graphite and commercial Pt/C electrocatalysts. This is due to covalently bonded sulfur, or oxidized sulfur, at the edge of graphene that induced both charge and spin densities on the graphene. This was because the charge polarization stemming from

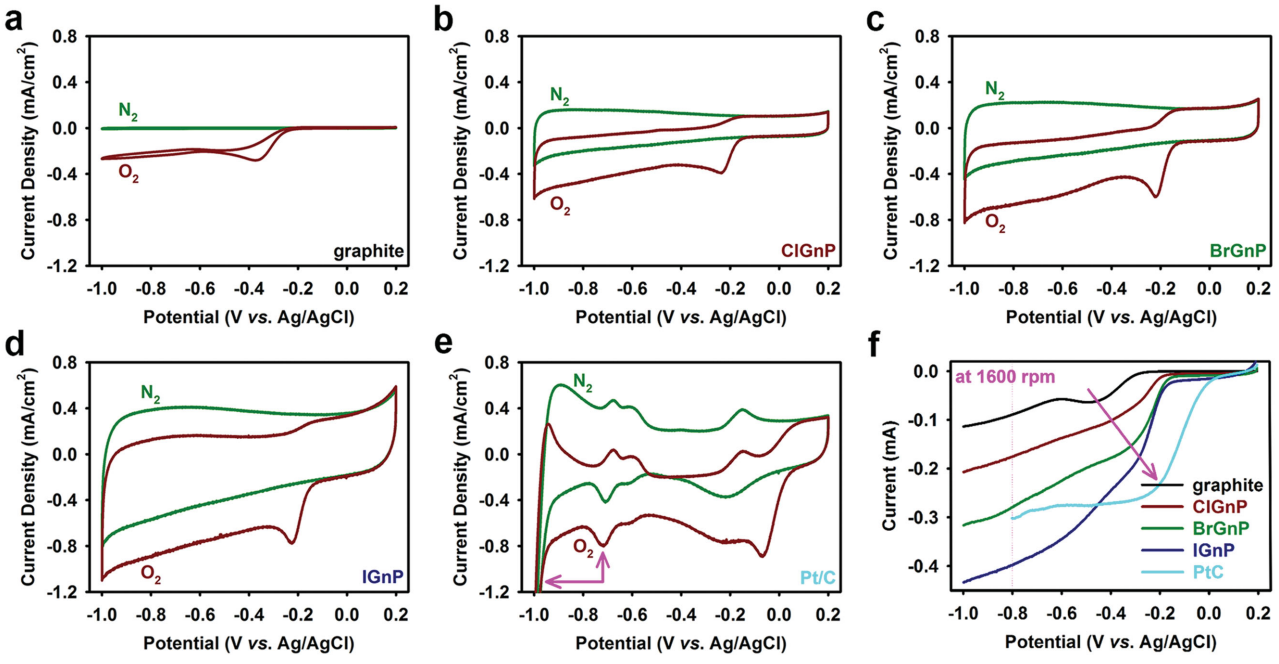

Figure 3. Cyclic voltammograms (CV) of XGnPs (X = Cl, Br, I) and Pt/C on glassy carbon (GC) electrodes in N_2- and O_2-saturated 0.1 M aq. KOH solution with a scan rate of 10 mV/s: a) Pristine graphite, b) ClGnPs, c) BrGnPs, d) IGnPs, and e) Pt/C; f) Linear sweep voltammograms (LSV) at a rotation rate of 1600 rev min^{-1} and a scan rate of 10 mV s^{-1}, showing a gradual increase in current and a positive shift in the onset potential along the order of the pristine graphite, ClGnPs, BrGnPs, IGnPs and Pt/C. Reproduced with permission.[27] Copyright 2013, Nature Publishing Group.

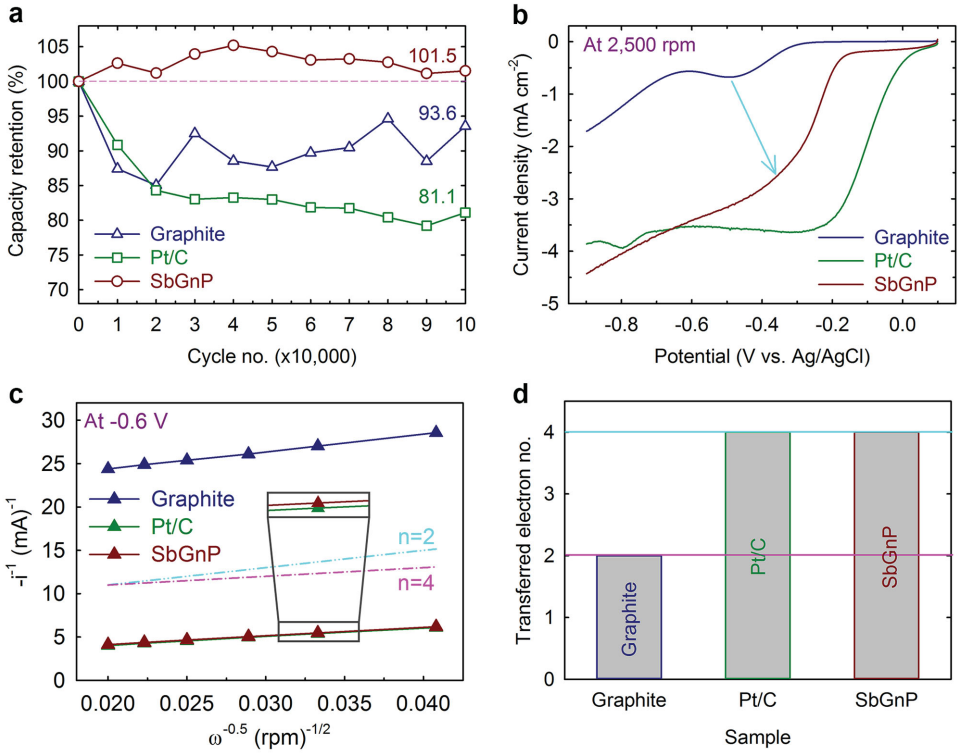

Figure 4. Electrochemical analysis of pristine graphite, Pt/C, and SbGnPs: a) Capacity retention in an O_2-saturated 0.1 M aq. KOH solution with a scan rate of 100 mV s^{-1}, illustrating that SbGnPs displayed no capacity loss after 100 000 cycles; b) Linear sweep voltammograms (LSVs) at a rotation rate of 2500 rpm and a scan rate of 10 mV s^{-1}; c) Koutecky-Levich plots derived from the rotating disk electrode measurements at 0.6 V; d) The electron transfer number at 0.6 V (versus Ag/AgCl).Reproduced with permission.[31] Copyright 2015, Nature Publishing Group.

the difference in electronegativity between carbon (χ = 2.55) and sulfur (χ = 2.58) is almost negligible. Specifically, they are strongly polarized by the covalently bonded sulfur atoms at the edge of the graphene and there, the polarized zones should serve as active sites for ORR. Additionally, SOGnPs show better electrocatalytic activity than SGnPs-S_8 due to their higher magnetic moment (related to electron motion and transfer).

Antimony-doped graphene nanoplatelets (SbGnPs) are prepared directly by ball-milling graphite in the presence of antimony (Sb).[31] Due to antimony doping, SbGnPs show the cathodic reduction peak more positively (≈0.13 V, compared with that of pristine graphite) but manifests high electrocatalytic activity. The current density of SbGnPs was almost 3-fold greater than that of pristine graphite, and equivalent to commercial Pt/C. The experimentally determined n value at the potential of –0.6 V (for both SbGnPs and Pt/C) exhibits an ideal one-step, four-electron pathway (n = 4.0), while the electron pathway of pristine graphite shows the classic two-electron pathway (n = 2.0) for ORR. For the tolerance against CO poisoning and methanol crossover, SbGnPs also displayed performance superior to that of pristine graphite and Pt/C. More importantly, SbGnPs displayed zero loss of electrocatalytic activity for ORR, even after 100 000 cycles. Density functional theory (DFT) calculations indicate that the multiple oxidation states (Sb^{3+} and Sb^{5+}) of Sb are responsible for this unusual electrochemical stability (**Figure 4**). The free energy profile is favorable along the ORR paths through intermediates that alternate between the multiple oxidation states of Sb. Furthermore, the dissociative processes are preferred to the associative ones, and thus the formation of hydrogen peroxide (H_2O_2) is suppressed during the ORR process, supporting the observed cycle stability.

Iodine[27] and sulfuric acid[26] functionalized GnPs showed outstanding properties as electrocatalysts for ORR. Expecting synergistic enhancement, iodine/sulfonic acid co-doped GnPs (ISGnPs) were prepared by sequential ball-milling to use high charge polarization for iodine and high polarity for -SO_3H.[30] Despite low surface area (6.03 m^2 g^{-1}), the ISGnPs showed significantly improved onset potential for ORR, compared to pristine graphite and hydrogen-functionalized GnPs (HGnPs, low grain-size GnPs). The electron transfer number (n) of ISGnPs increased from 2.8 to 4.0 as the applied potential increased from –0.4 to –0.6 V, which is a typical potential range of fuel cell operation, indicating that ISGnPs contribute to efficient oxygen diffusion and absorption. The introduction of iodine (I) and sulfonic acid (–SO_3H) at the edge of graphitic layers was found to produce good ORR performance with higher capacitance and better cycle stability than commercial Pt/C electrocatalyst.

6.2. As Counter Electrode Materials for Dye-Sensitized Solar Cells (DSSCs)

Dye-sensitized solar cells (DSSCs), which were first developed about two decades ago, are considered to be potential alternatives to current silicon-based solar cells. The advantages of DSSCs are low-cost, dye availability, easy fabrication, and high

power conversion efficiency (PCE).[56,57] The key roles of the counter electrode (CE) in DSSCs are to rapidly transfer electrons from the external circuit to the electrolyte and to efficiently catalyze the reduction of the redox couple. Hence, the requirements for efficient CEs include good charge-transfer properties due to low sheet resistance and efficient catalytic reduction, via charge polarization, of the redox couple.[58] Thus far, Pt is one of the best catalysts that meet these requirements, for use in fuel cells. As aforementioned, Pt is an expensive and scarce noble metal and is subject to corrosion. Therefore, carbon-based materials, such as carbon black,[59] carbon nanoparticles,[60] carbon nanotubes,[61] and graphene,[62,63] have been widely studied in hopes of finding promising alternatives to replace Pt-based materials. We have tested EFGnPs as CEs and they show good electrocatalytic performance for the $Co(bpy)_3^{2+/3+}$ redox couple, and lower charge-transfer resistance (R_{ct}) values at the CE/electrolyte interface. In particular, the electrochemical stability of EFGnP-CE for the $Co(bpy)_3^{2+/3+}$ redox couple is profoundly better than that of the Pt-CE (**Table 6**).

For example, the NGnP-based DSSC shows a J_{SC} of 14.78 mA cm^{-2}, a V_{OC} of 966 mV, a FF of 71.9% and a PCE of 10.27%.[36] For comparison, the Pt-based DSSC was also tested, showing a J_{SC} of 14.57 mA cm^{-2}, a V_{OC} of 970 mV, a FF of 70.5% and a PCE of 9.96% (Table 6 and **Figure 5**). The NGnP-based DSSC displayed higher J_{SC} and FF than those of the Pt-based DSSC. The result can be attributed to the low R_{ct} at the CE/electrolyte interface, resulting in enhanced DSSC performance. The enhanced performance of the NGnPs-CEs can be ascribed to efficient charge polarization due to the high level (≈11 at.%) of edge-selective nitrogen-doping, and to the good charge transfer resulting from low sheet-resistance, which originates from the high degree of crystallinity of EFGnPs on their basal plane. These results support the important role of carbon-based, metal-free CEs in DSSCs. Furthermore, the electrochemical stability of the NGnP-CE for the $Co(bpy)_3^{2+/3+}$ redox couple, is much better than of the Pt-CE.

Table 6. Photovoltaic performance of EFGnPs for DSSC.

Sample	J_{SC} [mA cm^{-2}]	V_{OC} [mV]	FF [%]	PCE [%]	Reference
Pt/C	14.24 ± 0.28	974 ± 4.2	70.6 ± 1.1	9.92 ± 0.12	[35]
HGnP	14.05 ± 0.08	925 ± 8.7	45.8 ± 0.13	5.96 ± 0.01	[32
CGnP	14.06 ± 0.16	889 ± 1	74.4 ± 0.9	9.31 ± 0.03	33
NGnP	14.78	866	71.9	10.27	[34]
FGnP	14.44 ± 0.03	962 ± 1.1	71.5 ± 0.35	10.01 ± 0.06	[32]
ClGnP	14.40 ± 0.25	962 ± 4	69.2 ± 2.5	9.58 ± 0.15	[35]
BrGnP	14.59 ± 0.13	974 ± 3	71.6 ± 0.6	10.03 ± 0.13	[35]
IGnP	14.81 ± 0.34	977 ± 4	71.3 ± 1.1	10.31 ± 0.11	[35]

Carboxylic acid-functionalized GnPs (CGnPs) were tested as CEs in a DSSC. They showed much lower R_{ct} (0.87 Ω cm^2) and better electrochemical stability under prolonged cycling potential than did a Pt-CE (2.19 Ω cm^2). The other values of the DSSC with the CGnP-CE were J_{SC}, V_{OC}, FF, and PCE of 14.07 mA cm^{-2}, 889 mV, 74.4%, and 9.31%, respectively. The values were much better than those (13.69 mA cm^{-2}, 877 mV,

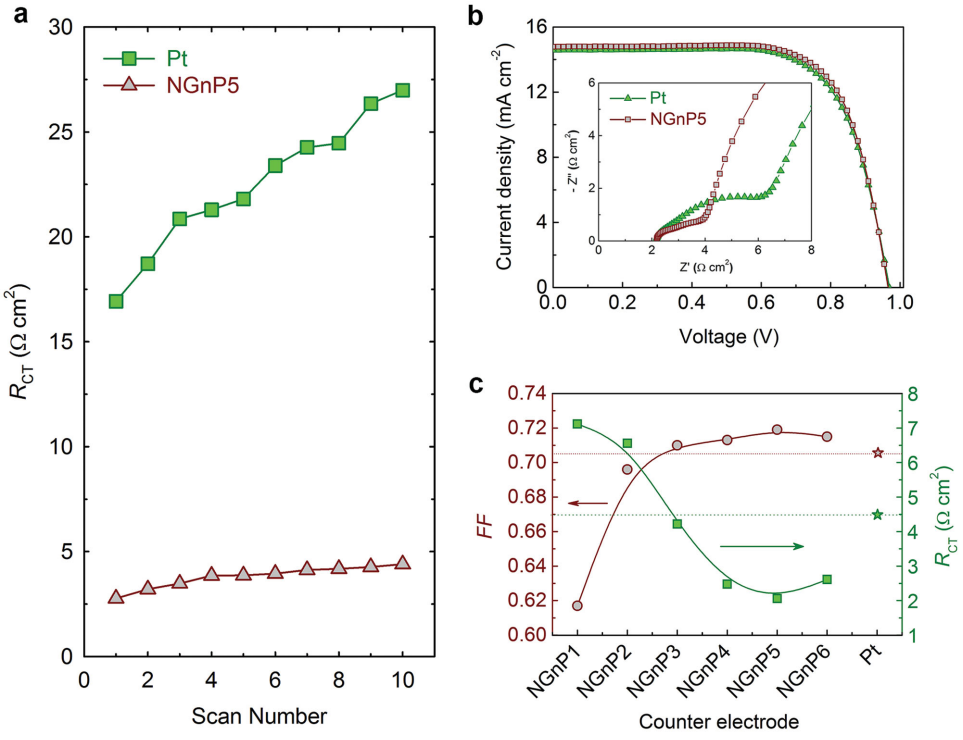

Figure 5. a) R_{CT} changes of the Pt and NGnP-CEs versus the EIS scan number, (b) Current-voltage characteristics of the DSSCs with Pt and the NGnP5 CEs under one-sun illumination (AM 1.5). The TiO_2 film thickness is 8.5 (5.5 + 3) μm and the active area (defined by a black metal mask) is 0.16 cm^2. The inset shows the Nyquist plots in the high frequency region of the DSSCs at a forward bias of -0.95 V under dark conditions. (c) FF and R_{ct} values for the DSSCs containing the various CEs.[34]

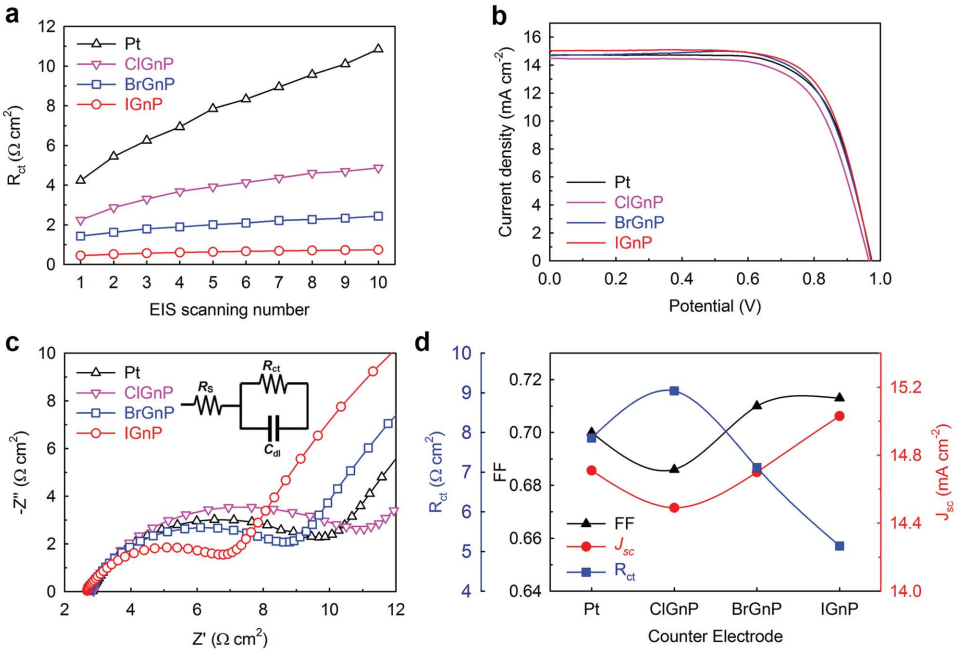

Figure 6. a) Variation of R_{ct} of Pt and XGnP-CEs versus EIS scan number, b) Current-voltage curves of DSSCs with various CEs under one-sun illumination (AM 1.5G). The TiO_2 film thickness is 8 (5 + 3) and active area (defined by a black metal mask) is 0.16 cm^2. c) Nyquist plots in the high-frequency region of the DSSCs at a forward bias of –0.95 V under dark conditions. d) Comparison of FF, J_{SC}, and R_{ct} for DSSCs with Pt-CE, and various XGnP-CEs. Reproduced with permission.[35] Copyright 2015, Elsevier.

68.7%, and 8.25%) of the corresponding DSSC with the Pt-CE (Table 6).[33]

In the case of halogen-doped GnPs (XGnPs, X = Cl, Br or I) in comparison with Pt, the R_{ct} values were 4.23, 2.24, 1.44, and 0.46 Ω cm^2 for the Pt-, ClGnP-, BrGnP- and IGnP-CE, respectively, in the first cycle, and 10.86, 4.87, 2.44, and 0.76 Ω cm^2 in the final cycle.[35] However, there were no noticeable changes in the low frequency region, indicating that the $Co(bpy)_3^{2+/3+}$ was stable, even with severe external cycling potentials. The DSSC with ClGnP-CE showed a J_{SC} of 14.40 mA cm^{-2}, a V_{OC} of 962 mV, an FF of 69.2%, and a PCE of 9.58%. The DSSC with a BrGnP-CE showed an even higher performance, with a J_{SC} of 14.59 mA cm^{-2}, a V_{OC} of 974 mV, an FF of 71.6%, and a PCE of 10.03% compared with the Pt-CE (J_{SC} 14.42 mA cm^{-2}; V_{OC} 975 mV; FF 70.6%; and PCE 9.92%). The DSSC with the IGnP-CE showed the best performance with J_{SC} of 14.81 mA cm^{-2}, V_{OC} of 977 mV, FF of 71.3%, and a PCE of 10.31% (Table 6 and **Figure 6**).

Due to the dangerous nature of fluorine (F_2) gas, handling it in an ordinary laboratory is not allowed. Recently, it was found that diluted F_2 gas (less than 20 vol%) in argon can be handled safely. Fluorine-doped graphene nanoplatelets (FGnPs) can be prepared by ball-milling in the presence of diluted F_2 gas. FGnP-CE displays even better electrocatalytic activity and electrochemical stability than those of the other XGnP-CEs (X = Cl, Br, I), and of the Pt-CE in $Co(bpy)_3^{2+/3+}$ medium.[32] The DSSC fabricated using the FGnP-CE exhibited higher photovoltaic performance (FF, J_{SC}, and PCE: 71.5%, 14.44 mA cm^{-2}, and 10.01%) than that with the Pt-CE (69.8%, 14.28 mA cm^{-2}, and 9.61%) (Table 6). The series resistance (R_s) and R_{ct} at the CEs/electrolyte interface of FGnP-CE are 2.24 and 0.47 Ω cm^2, respectively, whereas the corresponding values of Pt-CE are 2.27 and 1.87 Ω cm^2. The lower R_{ct} value for the FGnP-CE suggests high electrocatalytic activity for the reduction $Co(bpy)_3^{2+/3+}$ ions, which should enhance the DSSC performance.

6.3. As Anode Materials for Li-ion Batteries (LIBs)

Because of their high specific energy density and appreciable cycle life, Li-ion batteries (LIBs) are widely used energy storage devices used in a variety of portable and smart devices. As a commercial anode material in LIBs, graphite suffers from a relatively small capacity (372 mAh g^{-1}) and should be replaced by alternative anode materials with higher capacity and longer cycle life for commercial electric vehicles.[15,64] In order to enhance the reversible capacity of the electrode, there have been attempts to introduce defects, channels, and functional groups on the graphitic surface. It is now clear that it is important to develop carbon-based electrodes with enhanced charge polarization and stable chemical bonds, and to reduce the overpotentials for electrochemical reactions. This would make them less susceptible to corrosion of the oxidative electrode (e.g., $C + O_2 \rightarrow CO_2$). The halogen-doped GnPs (XGnPs), specifically X = F and I, have exhibited excellent electrochemical performance and enhanced cycle life in LIBs.

For example, an FGnPs anode was able to deliver an initial charge capacity of 650.3 mAh g^{-1} at 0.5 C and a voltage of 0.02–3 V, which are higher than for a conventional graphite-based electrode (a theoretical capacity of 372 mAh g^{-1}), and for the reference HGnPs with 511.3 mAh g^{-1}.[32] Even after 500 cycles, FGnPs anodes could still maintain a high capacity

Table 7. The initial capacity and capacity retention of EFGnPs for LIBs.

Sample	Initial Capacity [mAh g^{-1}]	Capacity retention (after 500 cycle)	Reference
Graphite	372 (theoretical capacity)	–	[65]
HGnP	511.3 (0.5 C)	40.8%	[36]
FGnP	650.3 (0.5 C)	76.6%	[32]
ClGnP	626.5 (0.5 C)	36.6%	[36]
BrGnP	546.8 (0.5 C)	38.5%	[36]
IGnP	562.8 (0.5 C)	81.4%	[36]

(498.2 mAh g^{-1}) with capacity retention of 76.6% (**Table 7**). The cycling performance of FGnPs are attributed to the higher electronegativity of fluorine (χ = 3.98) at the edges of FGnPs, creating a net positive charge on adjacent carbon atoms (χ = 2.55) that facilitates lithium extraction from/insertion into the electrode during cycling.

Other halogen series doped XGnPs (X = Cl, Br or I), and a reference hydrogen-doped GnPs (HGnPs), had initial charge capacities of 626.5 (ClGnP), 546.8 (BrGnP), 562.8 (IGnP), and 511.3 (HGnP) mAh g^{-1}, respectively, at 0.5 C in the voltage range of 0.02–3 V (Table 7 and **Figure 7**).[36] After 500 cycles, the sample cells delivered charge capacities of 229.5 (ClGnP), 210.6 (BrGnP), 458.0 (IGnP) and 208.5 (HGnP) mAh g^{-1}, with initial charge capacity retention of 36.6%, 38.5%, 81.4%, and 40.8%, respectively. The cycling performance of IGnPs is attributed to the large atomic size of iodine (I). Although the electronegativity of I (χ = 2.66) is the lowest in the halogen series, the covalent atomic radius of I (139 pm) is the largest among them, as well as being almost twice that of carbon (76 pm). The enlarged entrance of iodinated edges can more efficiently facilitate Li-ion insertion/extraction between graphitic layers. In addition, after 500 discharge/charge cycles and storage for one month under ambient conditions (25 °C), the IGnPs cell still showed a reversible capacity of 464.1 mAh g^{-1} at cycle 600. The outstanding cycling performance further indicates that IGnPs provide very stable and active anode materials for LIBs.

6.4. As Electrode Materials for Vanadium Redox-Flow Batteries (VRFBs)

Vanadium redox-flow batteries (VRFBs) have been considered as a promising large-scale stationary energy-storage system to alleviate issues of random and intermittent renewable energy sources currently in use.[66,67] Carbon-based catalysts such as carbon nanotubes (CNTs), carbon nanofibers (CNFs), and graphene are considered promising candidates due to their large surface area, good conductivity, and stability in concentrated acids.[68,69]

Carboxylic acid-functionalized GnPs (CGnPs) were tested as catalysts for VRFBs,[45] because the numerous oxygen atoms in the graphitic carbon frameworks assist the vanadium redox reactions.[70] The I_{pc}/I_{pa} ratio of CGnPs (ca. 0.9) is higher than for rGO (ca. 0.7), and the value of peak potential separation ($\Delta E = V_{pa}–V_{pc}$: 144 mV), associated with reversibility of CGnPs, is less than that of rGO (269 mV). The flow cell based on CGnPs showed an improved EE (EE = VE × CE) value,

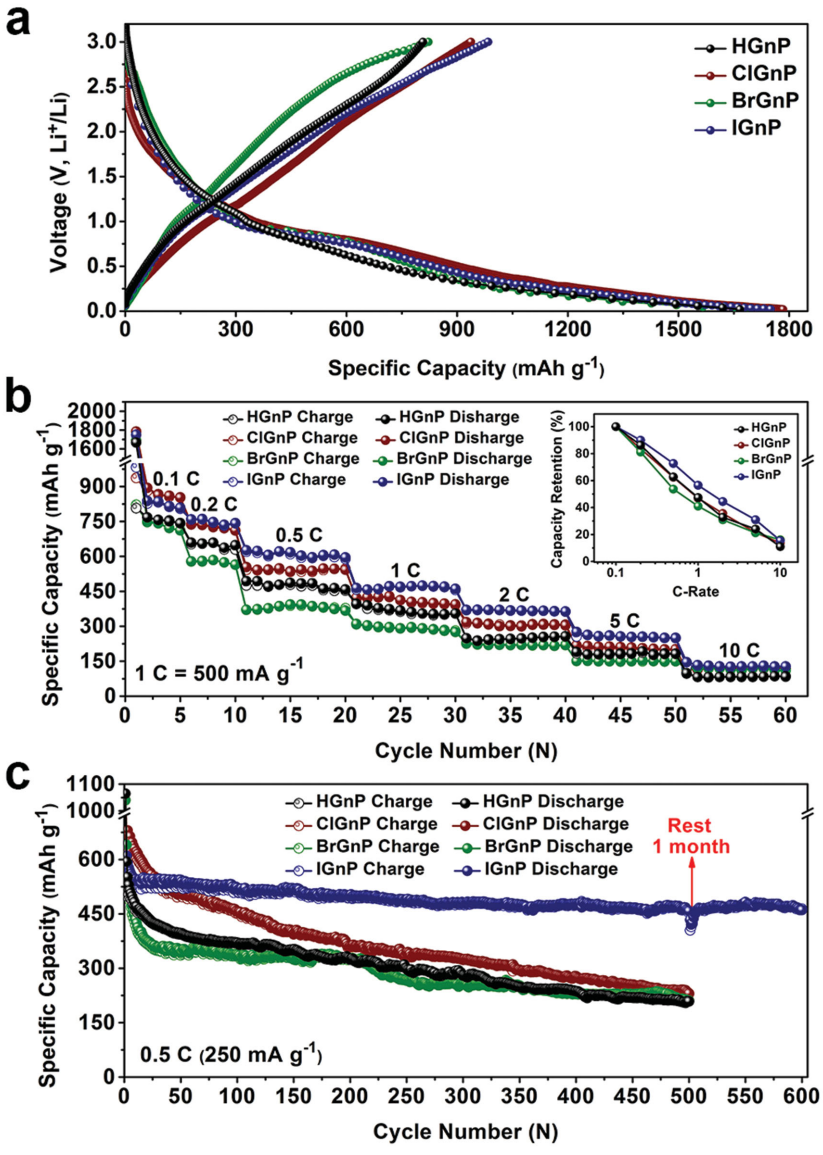

Figure 7. a) Initial discharge-charge curves at 0.1 C, b) Rate performance: Inset charge capacity retention at various current densities; c) cycling performance at 0.5 C of XGnP (X = H, Br, Cl or I) in the voltage range 0.02–3 V. The continued cycling performance of the IGnPs cell was obtained after 500 cycles and one month storage under ambient conditions (25 °C). Reproduced with permission.[36]

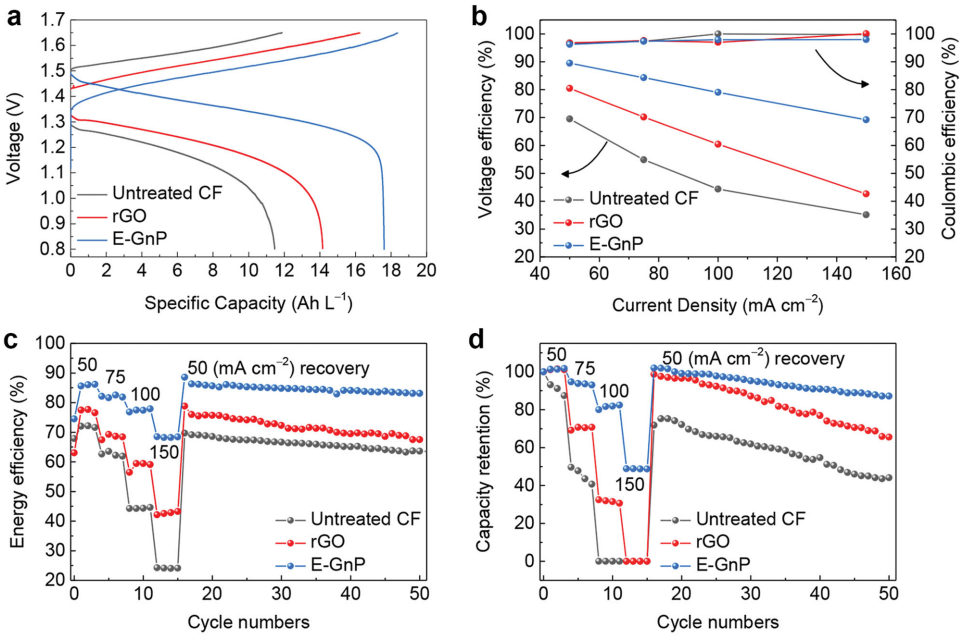

Figure 8. Electrochemical cycling performance of the untreated CF, rGO, and CGnP coated CF electrodes. a) Charge/discharge voltage profiles at a current density of 50 mA cm^{-2}; b) Coulombic and voltage efficiencies at different current densities ranging from 50–150 mA cm^{-2}. Rate capability tests: c) energy efficiency; d) capacity retention profiles of each electrode cycled at various current densities. Reproduced with permission.[45]

>15% higher than that of untreated carbon felt (CF), which is 5% higher than rGO at a current rate of 50 mA cm^{-2}. As the current density increased, there was no capacity retention in the rGO catalyst at over 150 mA cm^{-2}, while the CGnPs retained a substantially improved charge/discharge capacity. In addition, upon abruptly changing the current rate to 50 mA cm^{-2}, the original capacity of the CGnPs catalyst was almost recovered. The result implies stable cycling performance over 50 cycles (**Figure 8**). Therefore, the enhanced catalytic activity of CGnPs towards vanadium redox couples can be attributed to the defect-free basal plane for fast electron transfer and to abundant oxygen functional groups at the edges. It can be concluded that EFGnPs with edge-selective functionalization with various functional groups and/or heteroatoms that could efficiently promote the mass-transfer rate of the electrocatalyst used for vanadium redox-flow batteries (VRFBs), are advantageous for adsorption/desorption of the vanadium redox couples.

6.5. As Materials for Flame Retardants

Brominated flame retardants (BFRs) are currently used in various products to enhance fire safety. However, the usage patterns of current flame retardants are changing in light of their environmental hazard, exposure data, and new regulations. Due to their persistent nature, tendency to bioaccumulate, and toxic properties, the European Union (EU) and some US states have banned the use of pentabromodiphenyl ether (pentaBDE) and octabromodiphenyl ether (octaBDE).[46] Therefore, the phase-out of several high-production-volume BFRs calls for increased production and application of alternative flame retardants. Specifically, phosphorus-containing flame retardants have received tremendous attention due to their non-toxicity and eco-friendliness.

When phosphorous can be introduced at the edges of GnPs, the flame retardation/non-flammability would be maximized. By using the mechanochemical ball-milling method, the formation of C–P bonds at the edges of GnPs can be realized by ball-milling graphite in the presence of safe, red phosphorus.[37] Upon exposure to the moisture in air, the phosphorus at the edges of phosphorus-functionalized GnPs (PGnPs) spontaneously oxidize into graphene phosphonic acid (–PO_3H_2) (GPA). The important characteristics of GPA are that it disperses very well in neutral water (as high as 0.6 mg mL^{-1}), which is the highest solubility reported in the literature (GO = 0.1 mg mL^{-1}).[62] Together with water solubility, GPA is readily dispersible in most polar solvents even without physical agitation due to the polar nature of phosphonic acids. Aqueous GPA solution displays zeta-potential values of –40.4, –46.5, and –33.3 mV at concentrations of 0.40, 0.50, and 0.60 mg mL^{-1}, respectively. An aqueous GPA solution is simply coated onto a piece of paper (mulberry paper, hanji) to test the flame retardation. While the hanji without GPA coating completely burned in 10 s, leaving traces of white ash, the GPA-coated hanji emitted white smoke (moisture vaporization) in the beginning without catching fire and maintained the initial shape with little shrinkage (**Figure 9**). GPA exhibits outstanding performance as a fire retardant by physical retardation. This is related to the cooling of the burning surface by endothermic reaction and vaporization (fuel cooling). It also exhibits chemical retardation, which is related to the thermal condensation of phosphonic acid to form char on the surface of a solid fuel (hanji) thus blocking the fuel supply. The results demonstrate that GPA will be useful as alternative flame retardants and should come to play key roles in flame retardation for the first time.

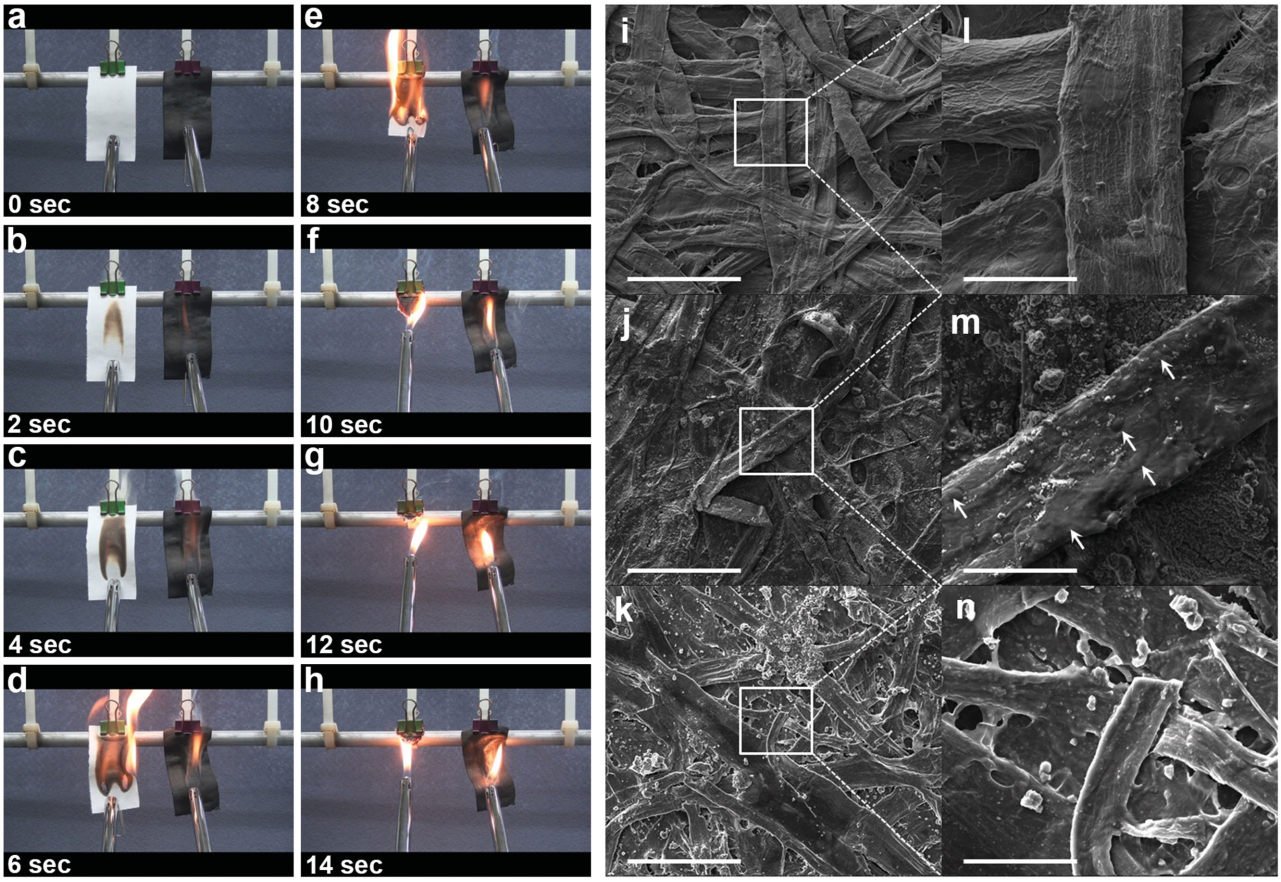

Figure 9. a–h) Snapshot of flame results of mulberry paper (left) and GPA/mulberry paper (right) with respect to time in seconds, i–n) SEM images at different magnifications: i, l) mulberry paper; j, m) GPA/Mulberry paper; k, n) flame results of untreated and GPA-treated Mulberry paper. The scale bars are 100 μm (i, j, k) and 20 μm (l, m, n). Reproduced with permission.[37] Copyright 2014, American Chemical Society.

7. Summary

In the near future, graphene is expected to begin fulfilling its outstanding potential and lead to greener, more efficient, and more economical materials for various applications. However, the existing major approaches, such as CVD and GO/rGO, have failed to demonstrate adequate commercialization potential to meet the market demand for diverse uses. Reasons for this include limiting factors such as high-cost, low-quality, poor producibility, environmental issues, and/or complicated tedious processes. Hence, there must be innovation to overcome current technological obstacles. We believe edge-selective functionalized graphene nanoplatelets (EFGnPs) could be the answer. The approach is a very simple, efficient, eco-friendly, and low-cost method for mass production. This method utilizes mechanical force (kinetic energy) to activate carbon species, which can then react with various chemical species to form C–X bonds at the broken edges of GnPs. In this way, the crystallinity on the GnP basal plane can be preserved to minimally scarify the outstanding natural properties of graphene. The method is considered to be one of the most powerful ways to achieve edge-selective formation of graphitic C–X bonds, including those with nonmetals, semimetals, and metalloids. As a result, EFGnPs can be used for many different applications and already show outstanding performance in energy conversion and storage, and as flame retardants. This is because mechanochemical reactions can maintain the intrinsic excellent properties of graphitic structure by edge-selective functionalization. Furthermore, due to the availability of customizable edge-functional groups in EFGnPs, new potential applications are unlimited. Tailoring edge groups is possible simply by changing reactants. The properties of the EFGnPs can be tuned to meet the specific demands of various applications, which is very difficult or impossible using the CVD or GO/rGO approaches. Therefore, EFGnPs have a number of advantages over conventional techniques for graphene production such as simplicity, low-cost, high-quality, tunable nature, and mass producibility. This technology has been transferred to industry and EFGnPs will begin to appear in the market. We anticipate a broad range of applications from wet chemistry to device applications, and to this process being recognized in the near future, as a method for mass production of GnPs for next generation materials. Hence, the mechanochemical ball-milling approach will contribute to significant advances in materials science and technology. Remaining challenges are controlling edge-functionality and grain size with respect to reactants and milling conditions, imparting more specific functionality for widening applications of EFGnPs.

Acknowledgements

This research was supported by the Creative Research Initiative (CRI), Mid-Career Researcher (MCR), BK21 Plus, the Basic Research Laboratory (BRL) programs through the National Research Foundation (NRF) of Korea, and the US Air Force Office of Scientific Research through the Asian Office of Aerospace R&D (AFOSRAOARD).

Received: May 30, 2015
Revised: July 21, 2015
Published online: October 23, 2015

[1] K. S. Novoselov, A. K. Geim, S. V. Morozov, D. Jiang, Y. Zhang, S. V. Dubonos, I. V. Grigorieva, A. A. Firsov, *Science* **2004**, *306*, 666.
[2] K. S. Novoselov, A. K. Geim, S. V. Morozov, D. Jiang, M. I. Katsnelson, I. V. Grigorieva, S. V. Dubonos, A. A. Firsov, *Nature* **2005**, *438*, 197.
[3] Y. B. Zhang, Y. W. Tan, H. L. Stormer, P. Kim, *Nature* **2005**, *438*, 201.
[4] A. K. Geim, K. S. Novoselov, *Nat. Mater.* **2007**, *6*, 183.
[5] T. Ramanathan, A. A. Abdala, S. Stankovich, D. A. Dikin, M. Herrera-Alonso, R. D. Piner, D. H. Adamson, H. C. Schniepp, X. Chen, R. S. Ruoff, S. T. Nguyen, I. A. Aksay, R. K. Prud'Homme, L. C. Brinson, *Nat. Nanotechnol.* **2008**, *3*, 327.
[6] S. Stankovich, D. A. Dikin, G. H. B. Dommett, K. M. Kohlhaas, E. J. Zimney, E. A. Stach, R. D. Piner, S. T. Nguyen, R. S. Ruoff, *Nature* **2006**, *442*, 282.
[7] S. Bae, H. Kim, Y. Lee, X. Xu, J.-S. Park, Y. Zheng, J. Balakrishnan, T. Lei, H. Ri Kim, Y. I. Song, Y.-J. Kim, K. S. Kim, B. Özyilmaz, J. H. Ahn, B. H. Hong, S. Iijima, *Nat. Nanotechnol.* **2010**, *5*, 574.
[8] K. S. Kim, Y. Zhao, H. Jang, S. Y. Lee, J. M. Kim, K. S. Kim, J. H. Ahn, P. Kim, J.-Y. Choi, B. H. Hong, *Nature* **2009**, *457*, 706.
[9] I. Meric, M. Y. Han, A. F. Young, B. Ozyilmaz, P. Kim, K. L. Shepard, *Nat. Nanotechnol.* **2008**, *3*, 654.
[10] X. Wang, L. Zhi, K. Müllen, *Nano Lett.* **2008**, *8*, 323.
[11] Z. Yin, S. Wu, X. Zhou, X. Huang, Q. Zhang, F. Boey, H. Zhang, *Small* **2010**, *6*, 307.
[12] L. Qu, Y. Liu, J. -B. Baek, L. Dai, *ACS Nano* **2010**, *4*, 1321.
[13] Q. Li, S. Zhang, L. Dai, L. S. Li, *J. Am. Chem. Soc.* **2012**, *134*, 18932.
[14] Z. S. Wu, W. Ren, L. Wen, L. Gao, J. Zhao, Z. Chen, G. Zhou, F. Li, H. M. Cheng, *ACS Nano* **2010**, *4*, 3187.
[15] E. Yoo, J. Kim, E. Hosono, H. S. Zhou, T. Kudo, I. Honma, *Nano Lett.* **2008**, *8*, 2277.
[16] F. Schedin, A. K. Geim, S. V. Morozov, E. W. Hill, P. Blake, M. I. Katsnelson, K. S. Novoselov, *Nat. Mater.* **2007**, *6*, 652.
[17] M. D. Stoller, S. Park, Y. Zhu, J. An, R. S. Ruoff, *Nano Lett.* **2008**, *8*, 3498.
[18] N. Behabtu, J. R. Lomeda, M. J. Green, A. L. Higginbotham, A. Sinitskii, D. V. Kosynkin, D. Tsentalovich, A. N. G. Parra-Vasquez, J. Schmidt, E. Kesselman, Y. Cohen, Y. Talmon, J. M. Tour, M. Pasquali, *Nat. Nanotechnol.* **2010**, *5*, 406.
[19] S. Park, R. S. Ruoff, *Nat. Nanotechnol.* **2009**, *4*, 217.
[20] S. Stankovich, D. A. Dikin, R. D. Piner, K. A. Kohlhaas, A. Kleinhammes, Y. Jia, Y. Wu, S. T. Nguyen, R. S. Ruoff, *Carbon* **2007**, *45*, 1558.
[21] D. A. Dikin, S. Stankovich, E. J. Zimney, R. D. Piner, G. H. B. Dommett, G. Evmenenko, S. T. Nguyen, R. S. Ruoff, *Nature* **2007**, *448*, 457.
[22] Z.-S. Wu, W. Ren, L. Gao, J. Zhao, Z. Chen, B. Liu, D. Tang, B. Yu, C. Jiang, H.-M. Cheng, *ACS Nano* **2009**, *3*, 411.
[23] C. Berger, Z. Song, X. Li, X. Wu, N. Brown, C. Naud, D. Mayou, T. Li, J. Hass, A. N. Marchenkov, E. H. Conrad, P. N. First, W. A. de Heer, *Science* **2006**, *312*, 1191.
[24] X. Li, W. Cai, J. An, S. Kim, J. Nah, D. Yang, R. Piner, A. Velamakanni, I. Jung, E. Tutuc, S. K. Banerjee, L. Colombo, R. S. Ruoff, *Science* **2009**, *324*, 1312.
[25] I.-Y. Jeon, Y.-R. Shin, G.-J. Sohn, H.-J. Choi, S.-Y. Bae, J. Mahmood, S.-M. Jung, J.-M. Seo, M.-J. Kim, D. W. Chang, L. Dai, J.-B. Baek, *Proc. Natl. Acad. Sci. U.S.A.* **2012**, *109*, 5588.
[26] I.-Y. Jeon, H.-J. Choi, S.-M. Jung, J.-M. Seo, M.-J. Kim, L. Dai, J.-B. Baek, *J. Am. Chem. Soc.* **2013**, *135*, 1386.
[27] I.-Y. Jeon, H.-J. Choi, M. Choi, J.-M. Seo, S.-M. Jung, M.-J. Kim, S. Zhang, L. Zhang, Z. Xia, L. Dai, N. Park, J.-B. Baek, *Sci. Rep.* **2013**, *3*, 1810.
[28] I.-Y. Jeon, H.-J. Choi, M. J. Ju, I. T. Choi, K. Lim, J. Ko, H. K. Kim, J. C. Kim, J.-J. Lee, D. Shin, S.-M. Jung, J.-M. Seo, M.-J. Kim, N. Park, L. Dai, J.-B. Baek, *Sci. Rep.* **2013**, *3*, 2260.
[29] I.-Y. Jeon, S. Zhang, L. Zhang, H.-J. Choi, J.-M. Seo, Z. Xia, L. Dai, J.-B. Baek, *Adv. Mater.* **2013**, *25*, 6138.
[30] J.-Y. Baek, I.-Y. Jeon, J.-B. Baek, *J. Mater. Chem. A* **2014**, *2*, 8690.
[31] I.-Y. Jeon, M. Choi, H.-J. Choi, S.-M. Jung, M.-J. Kim, J.-M. Seo, S.-Y. Bae, S. Yoo, G. Kim, H. Y. Jeong, N. Park, J.-B. Baek, *Nat. Commun.* **2015**, *6*, 7123.
[32] I.-Y. Jeon, M. J. Ju, J. Xu, H.-J. Choi, J.-M. Seo, M.-J. Kim, I. T. Choi, H. M. Kim, J. C. Kim, J.-J. Lee, H. K. Liu, H. K. Kim, S. Dou, L. Dai, J.-B. Baek, *Adv. Funct. Mater.* **2015**, *25*, 1170.
[33] M. J. Ju, I.-Y. Jeon, K. Lim, J. C. Kim, H.-J. Choi, I. T. Choi, Y. K. Eom, Y. J. Kwon, J. Ko, J. J. Lee, J.-B. Baek, H. K. Kim, *Energy Environ. Sci.* **2014**, *7*, 1044.
[34] M. J. Ju, I.-Y. Jeon, J. C. Kim, K. Lim, H.-J. Choi, S.-M. Jung, I. T. Choi, Y. K. Eom, Y. J. Kwon, J. Ko, J.-J. Lee, H. K. Kim, J.-B. Baek, *Adv. Mater.* **2014**, *26*, 3055.
[35] I.-Y. Jeon, H. M. Kim, I. T. Choi, K. Lim, J. Ko, J. C. Kim, H.-J. Choi, M. J. Ju, J.-J. Lee, H. K. Kim, J.-B. Baek, *Nano Energy* **2015**, *13*, 336.
[36] J. Xu, I.-Y. Jeon, J.-M. Seo, S. Dou, L. Dai, J.-B. Baek, *Adv. Mater.* **2014**, *26*, 7317.
[37] M.-J. Kim, I.-Y. Jeon, J.-M. Seo, L. Dai, J.-B. Baek, *ACS Nano* **2014**, *8*, 2820.
[38] D. Chen, H. Feng, J. Li, *Chem. Rev.* **2012**, *112*, 6027.
[39] D. R. Dreyer, S. Park, C. W. Bielawski, R. S. Ruoff, *Chem. Soc. Rev.* **2010**, *39*, 228.
[40] Y. Xu, Z. Liu, X. Zhang, Y. Wang, J. Tian, Y. Huang, Y. Ma, X. Zhang, Y. Chen, *Adv. Mater.* **2009**, *21*, 1275.
[41] H. J. Salavagione, M. A. Gómez, G. Martķnez, *Macromolecules* **2009**, *42*, 6331.
[42] D. H. Everett, *Basic Principles of Colloid Science*, Royal Society of Chemistry, London, UK **1988**, p. 76.
[43] D. Hanaor, M. Michelazzi, C. Leonelli, C. C. Sorrell, *J. Eur. Ceram. Soc.* **2012**, *32*, 235.
[44] K. Gong, F. Du, Z. Xia, M. Durstock, L. Dai, *Science* **2009**, *323*, 760.
[45] M. Park, I.-Y. Jeon, J. Ryu, J.-B. Baek, J. Cho, *Adv. Energy Mater.* **2015**, *5*, 1401550.
[46] S. H. Brandsma, J. de Boer, W. P. Cofino, A. Covaci, P. E. G. Leonards, *TrAC, Trends Anal. Chem.* **2013**, *43*, 217.
[47] A. B. Stambouli, *Renew. Sust. Energ. Rev.* **2011**, *15*, 1169.
[48] Y. Bing, H. Liu, L. Zhang, D. Ghosh, J. Zhang, *Chem. Soc. Rev.* **2010**, *39*, 2184.
[49] W. Sheng, H. A. Gasteiger, Y. Shao-Horn, *J. Electrochem. Soc.* **2010**, *157*, B1529.
[50] H. R. Byon, J. Suntivich, Y. Shao-Horn, *Chem. Mater.* **2011**, *23*, 3421.
[51] G. Wu, K. L. More, C. M. Johnston, P. Zelenay, *Science* **2011**, *332*, 443.
[52] L. Yang, S. Jiang, Y. Zhao, L. Zhu, S. Chen, X. Wang, Q. Wu, J. Ma, Y. Ma, Z. Hu, *Angew. Chem. Int. Ed.* **2011**, *123*, 7270.
[53] S. Wang, D. Yu, L. Dai, *J. Am. Chem. Soc.* **2011**, *133*, 5182.
[54] X. Sun, Y. Zhang, P. Song, J. Pan, L. Zhuang, W. Xu, W. Xing, *ACS Catal.* **2013**, *3*, 1726.

[55] T. Xing, J. Sunarso, W. Yang, Y. Yin, A. M. Glushenkov, L. H. Li, P. C. Howlett, Y. Chen, *Nanoscale* **2013**, *5*, 7970.
[56] B. O'Regan, M. Grätzel, *Nature* **1991**, *353*, 737.
[57] M. Grätzel, *Nature* **2001**, *414*, 338.
[58] J. D. Roy-Mayhew, D. J. Bozym, C. Punckt, I. A. Aksay, *ACS Nano* **2010**, *4*, 6203.
[59] T. N. Murakami, S. Ito, Q. Wang, M. K. Nazeeruddin, T. Bessho, I. Cesar, P. Liska, R. Humphry-Baker, P. Comte, P. Péchy, M. Grätzel, *J. Electrochem. Soc.* **2006**, *153*, A2255.
[60] R. Jia, J. Chen, J. Zhao, J. Zheng, C. Song, L. Li, Z. Zhu, *J. Mater. Chem.* **2010**, *20*, 10829.
[61] Z. Yang, T. Chen, R. He, G. Guan, H. Li, L. Qiu, H. Peng, *Adv. Mater.* **2011**, *23*, 5436.
[62] Y. Xu, H. Bai, G. Lu, C. Li, G. Shi, *J. Am. Chem. Soc.* **2008**, *130*, 5856.
[63] L. Kavan, J. H. Yum, M. Grätzel, *ACS Nano* **2011**, *5*, 165.
[64] J. Cabana, L. Monconduit, D. Larcher, M. R. Palacķn, *Adv. Mater.* **2010**, *22*, E170.
[65] S.-M. Paek, E. Yoo, I. Honma, *Nano Lett.* **2009**, *9*, 72.
[66] Z. Yang, J. Zhang, M. C. W. Kintner-Meyer, X. Lu, D. Choi, J. P. Lemmon, J. Liu, *Chem. Rev.* **2011**, *111*, 3577.
[67] B. Dunn, H. Kamath, J.-M. Tarascon, *Science* **2011**, *334*, 928.
[68] P. Han, Y. Yue, Z. Liu, W. Xu, L. Zhang, H. Xu, S. Dong, G. Cui, *Energy Environ. Sci.* **2011**, *4*, 4710.
[69] W. Li, J. Liu, C. Yan, *Carbon* **2013**, *55*, 313.
[70] W. Li, J. Liu, C. Yan, *Carbon* **2011**, *49*, 3463.